ELEVATED TEMPERATURE CRACK GROWTH*

S.N. Malik, R.H. Van Stone, K.S. Kim, J.H. Laflen
General Electric Company
Aircraft Engine Business Group
Cincinnati, Ohio

INTRODUCTION

Critical gas turbine engine hot section components such as blades, vanes, and combustor liners tend to develop minute cracks during the early stages of operation. These cracks may then grow under conditions of fatigue and creep to critical size. Current methods of predicting growth rates or critical crack sizes are inadequate, which leaves only two extreme courses of action. The first is to take an optimistic view with the attendant risk of an excessive number of service failures. The second is to take a pessimistic view and accept an excessive number of "rejections for cause" at considerable expense in parts and downtime. Clearly it is very desirable to develop reliable methods of predicting crack growth rates and critical crack sizes.

To develop such methods, it is necessary to relate the processes that control crack growth in the immediate vicinity of the crack tip to parameters that can be calculated from remote quantities, such as forces, stresses, or displacements. The most likely parameters appear to be certain path-independent (P-I) integrals, several of which have already been proposed for application to high temperature inelastic problems. A thorough analytical and experimental evaluation of these parameters needs to be made which would include elevated temperature isothermal and thermomechanical fatigue, both with and without thermal gradients.

In any investigation of fatigue crack growth, the problem of crack closure should be addressed in order to develop the appropriate crack growth model. Analytically, this requires the use of gap elements in a nonlinear finite element code to predict closure loads. Such predictions must be verified experimentally through detailed measurements; the best method for measuring crack closure has not been established in previous studies.

It is the purpose of this contract (NAS3-23940) to determine the ability of currently available P-I integrals to correlate fatigue crack propagation under conditions that simulate the turbojet engine combustor liner environment. The utility of advanced fracture mechanics measurements will also be evaluated and determined during the course of the program. These goals are to be accomplished through a two year, nine task, combined experimental and analytical program. To date an appropriate specimen design, a crack displacement measurement method, and boundary condition simulation in the computational model of the specimen has been achieved. Also, the experimental testing and data acquisition is continuing. Alloy 718 has been

*Work done under NASA Contract NAS3-23940.

selected as the analog material based on its ability to simulate high temperature behavior at lower temperatures in order to facilitate experimental measurements. Tensile and cyclic tests were run at several strain-rates so that an appropriate constitutive model could be developed. Available P-I integrals have been reviewed and the most suitable ones have been programmed into a finite element post-processor for eventual comparison with experimental data. These experimental data will include cyclic crack growth tests under thermo-mechanical conditions and, additionally, thermal gradients.

A REVIEW OF P-I INTEGRALS

The utility of the J integrals [1] as a parameter for predicting crack growth in the elastic-plastic regime is rather limited. The theoretical basis of the J integral does not allow the extension of its usage to nonproportional loading and unloading in the plastic regime, nor can it be utilized in the presence of a temperature gradient and material inhomogeneity. A typical example where all these limiting factors are operative would be the hot section components of a gas turbine in mission cycles.

In recent years there has been a considerable effort to modify and reformulate the J integral for applications in various areas of fracture mechanics. Consequently, a number of new path-independent (P-I) integrals have emerged in the literature. A critical review of these integrals is presented by Kim[2]. Notable among them are the Blackburn J*[3], Kishimoto $\hat{J}$[4, 5], Athuri ΔT_p and ΔT_p^*[6,7], and Ainswortn J_Θ[8] integrals. In the present program the theoretical background of these integrals has been examined with particular attention to whether or not the path-independence is maintained in the presence of nonproportional loading; unloading in the plastic regime; and a temperature gradient and material inhomogeneity. The relation among the P-I integrals, salient features and limitations were investigated. The physical meaning, the possibility of experimental measurements, and the computational ease were also examined. In view of the requirements associated with performing the tasks in this program the following conclusions were made.

i) The J^*, $\hat{J}$, ΔT_p and ΔT_p^* integrals maintain the path-independence under the thermomechanical cycles which will be used in the tests in this program and will be simulated numerically in subsequent tasks. Although the physical meaning of these P-I integrals needs to be further pursued, they would be the logical choices for further evaluation in this program.

ii) The J_Θ integral is a modified version of J to include thermal strain. Therefore, it cannot be used with substantially nonproportional loading and unloading in the plastic regime. It would be worthwhile, however, to investigate the utility of operationally defined J and possibly J_Θ for the test cycles in this program.

All selected P-I integrals have been implemented in a postprocessor to the General Electric nonlinear finite element program, CYANIDE. Numerical values of the integrals will be evaluated and examined for cracks subjected to various situations such as monotonic/cyclic loadings, unform/non-uniform temperature distributions, stationary/propagating cracks, etc. Best formulations suitable for all situations will be selected and used to correlate with the test results. The relationship between the analytical CTOD (or CMOD) displacements and the values of P-I integrals will be established to identify the displacement which must be measured to determine operational P-I integral.

EXPERIMENTAL PROGRAM

Alloy 718, a γ-γ'' nickel-base superalloy, has been selected as the analog material because over the temperature range from 800F to 1200F it shows very large changes in creep behavior. This permits the use of Alloy 718 to simulate the behavior of combustor liner materials while still performing experiments at relatively low temperatures. Tensile, creep, and cyclic constitutive tests have been performed on Alloy 718 over the temperature range from room temperature to 1200F to identify the constitutive properties to be used in finite element calculations. Tensile and cyclic tests have been performed over strain rates different by a factor of 20, and no strain rate sensitivity was observed, even at the higher temperatures where high creep rates occur. This will permit the use of classical plasticity and creep analysis in the Finite Element (FEM) analysis.

The primary specimen to be used in this study is a single edge crack (SEN) specimen with buttonhead grips. The buttonhead grips permit better load reversals and alignment, especially for compressive loads. The gage section has a rectangular cross-section with a thickness, width, and gage length of 2.54, 10.2 and 15.9mm (0.10, 0.40, and 0.625 inch) respectively. The relatively low gage length was selected to avoid buckling during the elevated temperature cycling with large plastic cyclic strains. The overall length of the specimen is 5 inch (127m) including the cylindrical shanks and buttonheads.

The SEN tests are performed in a strain control mode with the experimental setup shown schematically in Figure 1. The controlling extensometer will be mounted at the center of the 10.2mm wide surface of the specimen. Two other displacement gages, one to monitor crack mouth opening displacement (CMOD) and one to monitor the displacement on the face opposite the crack mouth, will also be used. The purpose of the CMOD gage is to detect when crack closure occurs. A standard 12.7mm (0.5 inch) elevated temperature extensometer has been modified to have a gage length of approximately 0.76mm (0.03 inch) and significantly improved resolution of CMOD displacements.

A DC potential drop system is used to monitor crack size. The load-displacement data is periodically recorded using an ETS data acquisition system. Figure 2 shows two examples of hysteresis loops obtained from typical

tests with $A_\varepsilon = \infty$ ($\varepsilon_{min} = -\varepsilon_{max}$). Figure 2a shows an example of nominally elastic cycling and a crack depth of approximately 0.51mm (20 mils). Even at this small crack length, the CMOD is detecting closure. Also note the displacement sensitivity of the CMOD loops is twice that of the other types of loops. Figure 2b shows an example of elastic-plastic strain cycling. The CMOD loop for this cycle shows crack closure and opening at very similar values of CMOD even though the nominal stress is much different due to net section plasticity. In both cases the back face extensometer shows a bias toward negative strains indicative of bending within the gage length.

The experimental work is in progress and will measure the crack growth response of Alloy 718 under isothermal, TMF, and temperature gradient conditions. Some additional tests were performed with a 12.7mm (0.5 inch) extensometer in place of the CMOD gage to provide verification of analytical results.

NUMERICAL COMPUTATIONS

Numerical implementation and verification of the PI-integral post-processor program was completed and is reported in the Annual Progress Report [9]. A pre-processor program for automatic generation of finite element two-dimensional meshes for crack problems was also completed and discussed in detail in the Annual Progress Report [9]. This mesh generator program allows a gradual transitioning of the elements size from relatively coarse in the remote stress field to very refined near the crack-tip region.

Prior to performing detailed FEM analyses for crack closure, efforts were made to evaluate simplified boundary conditions which would eliminate the need for analyzing the whole specimen (including the buttonhead). In order to verify the plane stress type stress field in the gage-section of the SEN specimen, a full-specimen three-dimensional (3D) analysis using 20-noded isoparametric brick elements was made by using the 3D-CYANIDE code. It was found that in the gage section there was very little variation in through-the-thickness stresses, strains, and displacements. Therefore, a 2D plane-stress model of the "full-specimen" was developed to investigate the influence of prescribed buttonhead displacements on the displacements in the "gage-section portion" of the specimen. Figure 3 shows the full-specimen model for the 2D-CYANIDE analysis which contains 566 nodes and 1002 constant strain elements. The near crack-tip mesh refinement was validated by prescribing constant displacement boundary conditions and computing stress intensity factor (K_I) from the post-processor J integral. For the elastic response, Figure 4 shows a comparison of computed K_I values with the Tada, Paris and Irwin handbook solution having a maximum difference of 7% for various a/w ratios. Similar comparisons made in the plastic regime using the elastic-plastic fracture mechanics handbook [10] solutions showed equally encouraging results.

The next step was to compare the computed load-displacement variation from the elastic-plastic analysis with the measured normal displacement data obtained from three 12.7mm (0.5 inch) extensometers positioned as shown in

Figure 1. Figures 5, 6 and 7 show the results obtained for an a/w ratio of 0.265. Solid lines represent test data curves for the first load cycle, whereas the circular symbols represent the computed values, and the square symbols represent test data for the second cycle. The monotonic stress-strain properties of Alloy 718 were used in the 2D-CYANIDE full-specimen analysis. It could be seen that the experimental first cycle load versus displacement data at each of the three extensometer locations compare very well with the computed values. The regions of extreme plasticity were modeled very satisfactorily by the 2D-CYANIDE analysis. Figure 8 shows u_y displacements, normal to the crack plane, near the end of gage-section. It could be seen that the u_y displacement varies approximately linearly across the gage-section width for all the seven load cases plotted in Figures 5, 6 and 7. For the larger displacement cases the u_y displacement near the back face (X = 0.4 inch) developed slight deviations from linearity. The most significant implication of Figure 8 is that due to linear variation of normal displacement across the specimen width near the end of the gage-section, only two extensometers are needed to accurately predict displacement response. This simplification eliminated the need for three extensometers needed to model gross specimen displacements.

Another interesting feature of the full-specimen 2D-CYANIDE analysis was the magnitude of horizontal displacement, u_x, in the gage-section. Figure 9 shows the relationship of the u_y versus u_x displacement at each of the nine x-coordinate locations near the end of gage-section for each of the seven load values plotted in Figures 5, 6 and 7. It could be seen that u_x displacement is about 30 to 60% of the corresponding u_y displacement at the end of gage-section.

Another simplification to reduce computer cost was made by only modeling the "gage-section portion" of the SEN buttonhead specimen. This gage-section model of the specimen retains the same mesh refinement as shown in Figure 3 except that the model is extended only up to 0.3125 inch (7.94mm). It now has only 359 nodes and 634 elements. This "gage-section portion" model was prescribed with zero u_x displacement at the top edge along which u_y displacements were applied either from the extensometer data or from the "full-specimen" 2D-CYANIDE solution (shown in Figures 5, 6 and 7). The extensometer data were taken only from the back-face (Figure 6) and middle-gage (Figure 5) and were linearly extrapolated to simulate the actual data acquisition from cyclic loading tests. Figures 10 and 11 show the results of the "gage-section" portion model driven by the experimental u_y data, and by the "full-specimen" extracted data, along with the full-specimen response. It could be seen that the elastic-plastic K_I values, in Figure 10, obtained from the post-processor J integral values for the full specimen and gage-section portion models are within 5% of each other. The induced vertical load in the gage-section model is within 8% of the full-specimen model, as shown in Figure 11. The experimental data driven gage-section portion model shows excellent agreement with the full-specimen analysis. These results were obtained for upper bound crack length to be used in this program, and it is felt that these conclusions will hold good for all the lower crack lengths.

CONCLUDING REMARKS

The work to date has shown that the 2D gage section modeling accurately simulates the behavior of the specimen as verified by experimental data. Work is continuing to simulate crack closure with the GAP-CYANIDE Finite Element Program. This effort along with the companion crack growth experiments will be used to identify path-independent integrals which predict the crack growth behavior under isothermal, TMF, and temperature gradient conditions.

REFERENCES

1. Rice, J.R., "A Path-Independent Integral and the Approximate Analysis of Strain Concentration by Notches and Cracks," Journal of Applied Mechanics, Vol. 35, 1968, pp. 379-386.

2. Kim, K.S., "A Review of Path-Independent Integrals in Elastic-Plastic Fracture Mechanics," General Electric Company, 1984, NASA Contractor Report; Also presented in ASTM 18th National Symposium on Fracture Mechanics, June 1985.

3. Blackburn, W.S., Jackson, A.D., and Hellen, T.K., "An Integral Associated With the State of a Crack Tip in a Nonelastic Material," International Journal of Fracture, Vol. 13, 1977, pp. 183-200.

4. Kishimoto, K., Aoki, S., and Sakata, M., "On the Path-Independent Integral-J," Engineering Fracture Mechanics, Vol. 13, 1980, pp. 841-850.

5. Aoki, S., Kishimoto, K., and Sakata, M., "Elastic-Plastic Analysis of Cracks in Thermally-Loaded Structures," Engineering Fracture Mechanics, Vol. 16, 1982, pp. 405-413.

6. Atluri, S.N., "Path-Independent Integrals, in Finite Elasticity and Inelasticity, With Body Forces, Inertia, and Arbitrary Crack-Face Conditions", Engineering Fracture Mechanics, Vol. 16, 1982, pp. 341-364.

7. Atluri, S.N., Nishioka, T., and Nakagaki, M., "Incremental Path-Independent Integrals in Inelastic and Dynamic Fracture Mechanics," Engineering Fracture Mechanics, Vol. 20, 1984, pp. 209-244.

8. Ainsworth, R.A., Neale, B.K., and Price, R.H., "Fracture Behavior in the Presence of Thermal Strains," Proceedings of Institute of Mechanical Engineers, Conference on Tolerance of Flaws in Pressurized Components, London, 1978, pp. 171-178.

9. Yau, J.F., Kim, K.S., Malik, S.N., Van Stone, R.H., and Laflen, J.H., "Elevated Temperature Crack Growth," Annual Progress Report, General Electric Company, NASA Contractor Report, 1985.

10. Kumar, V., German, M.D., and Shih, C.F., "An Engineering Approach for Elasto-Plastic Fracture Analysis," EPRI Report NP-1931 (R.P. 1237-1), Electric Power Research Institute, Palo Alto (CA.), 1981.

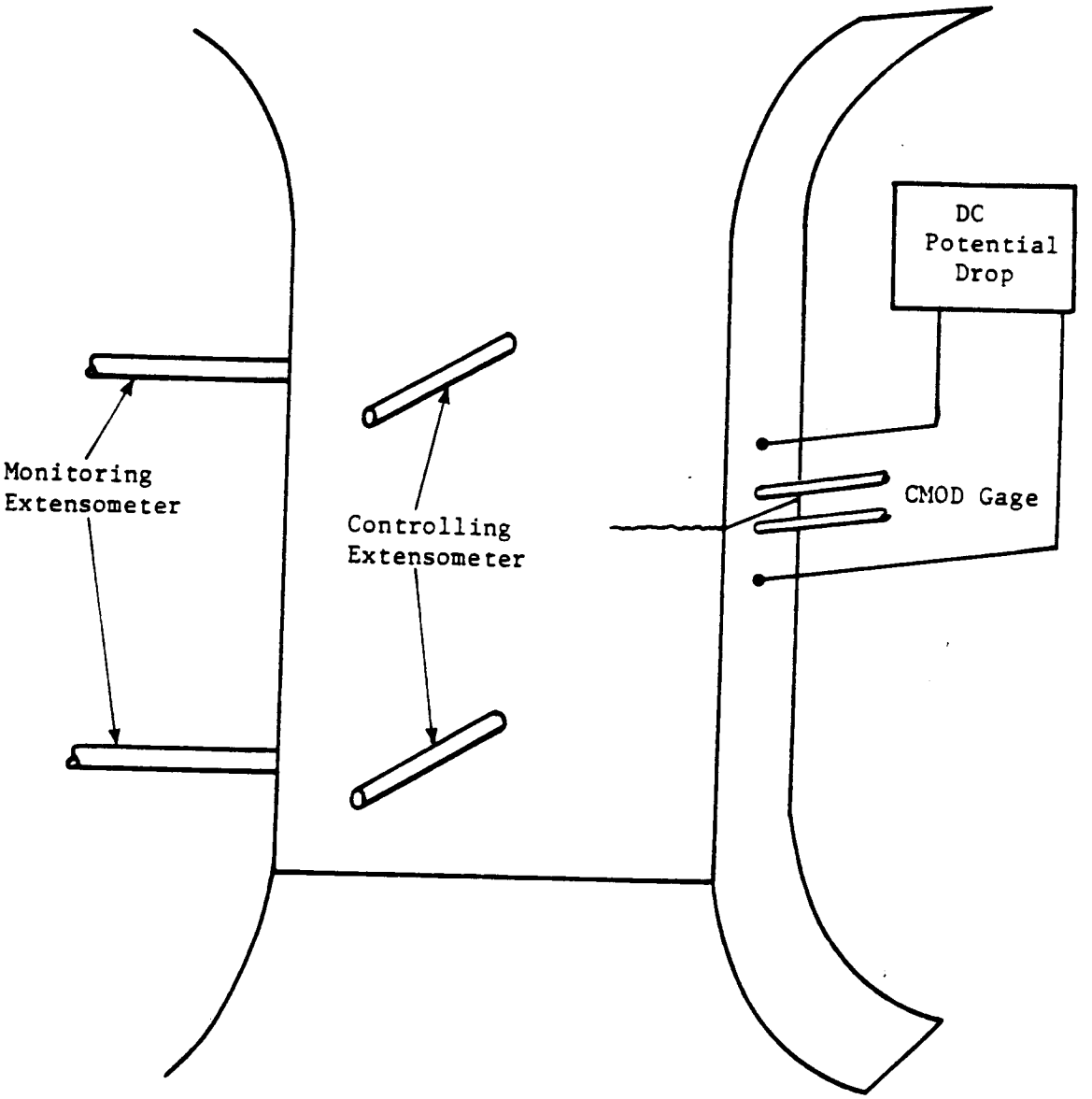

Figure 1. Schematic Drawing of SEN Test Method.

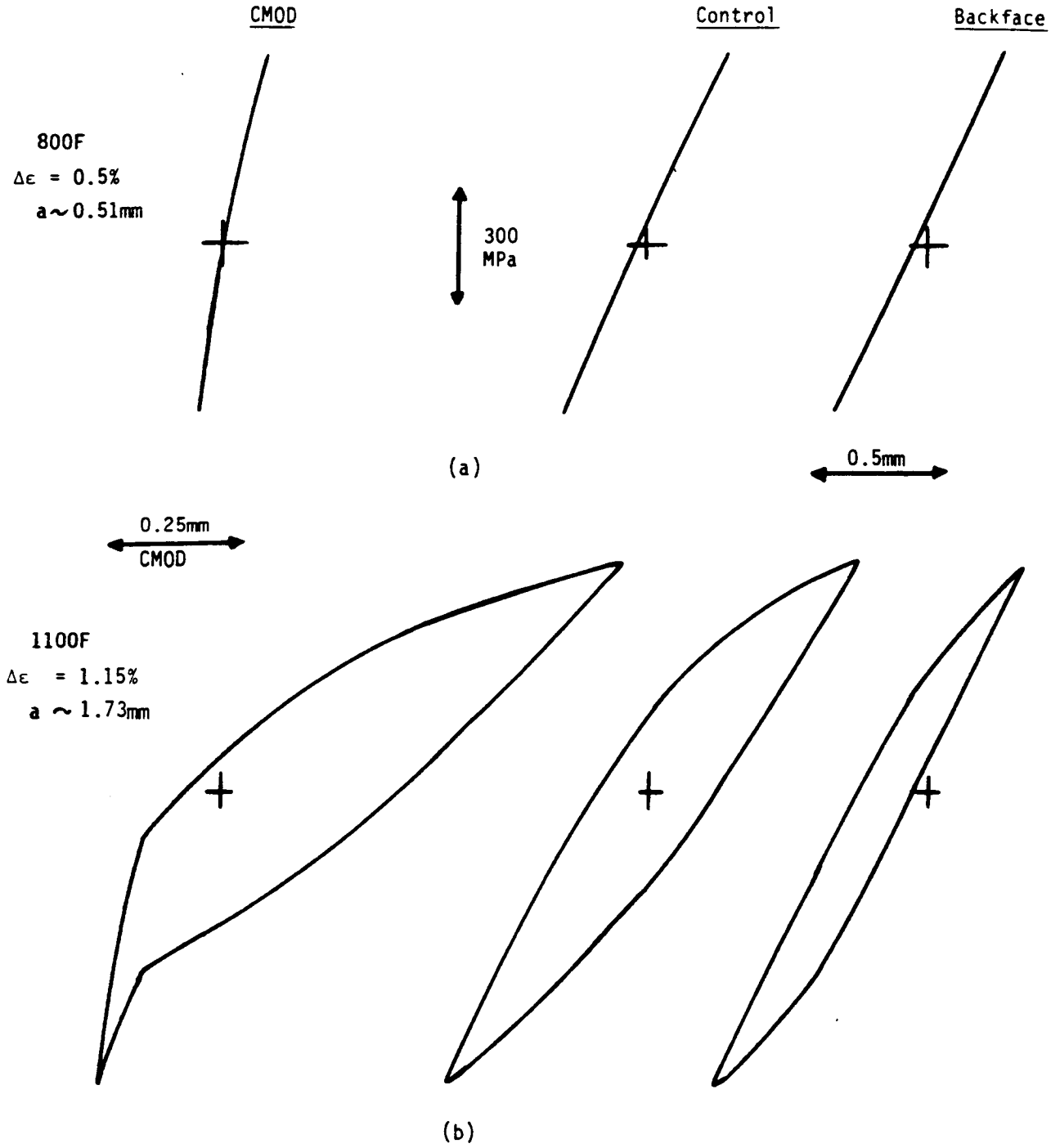

Figure 2: Examples of SEN Specimen Deflections Under (a) Elastic and (b) Elastic-Plastic

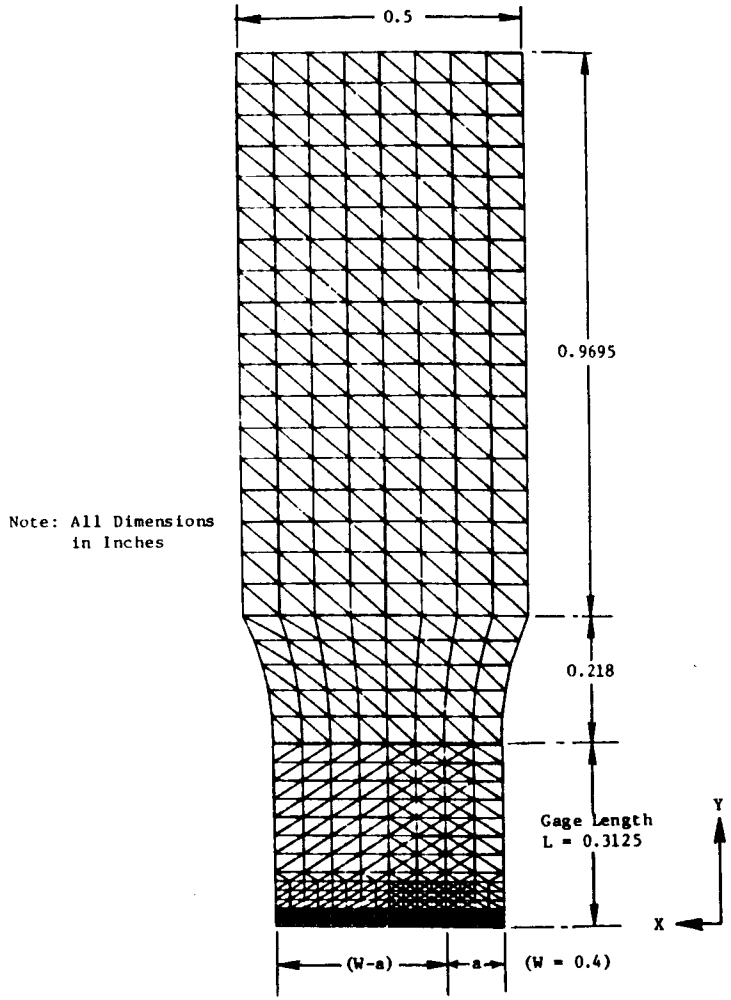

Figure 3. 2D Model of the SEN "Full Specimen" Including Gage-Length and Shank Portions.

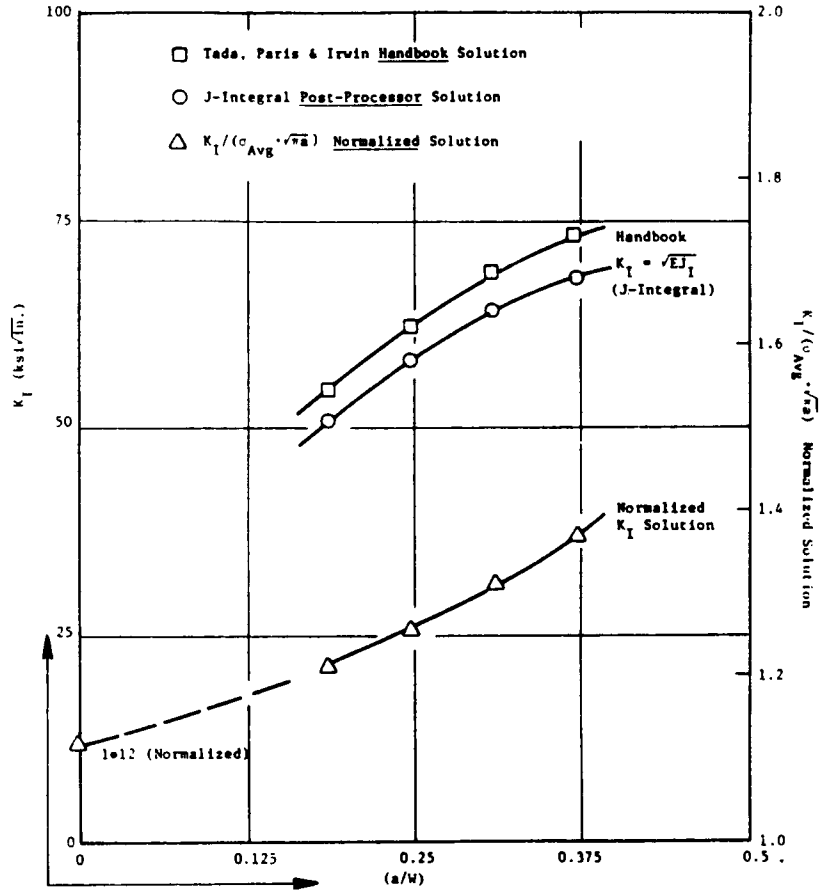

Figure 4. K_I Solution for SEN Specimen Subjected to a Uniform Normal Displacement at End of Gage Length.

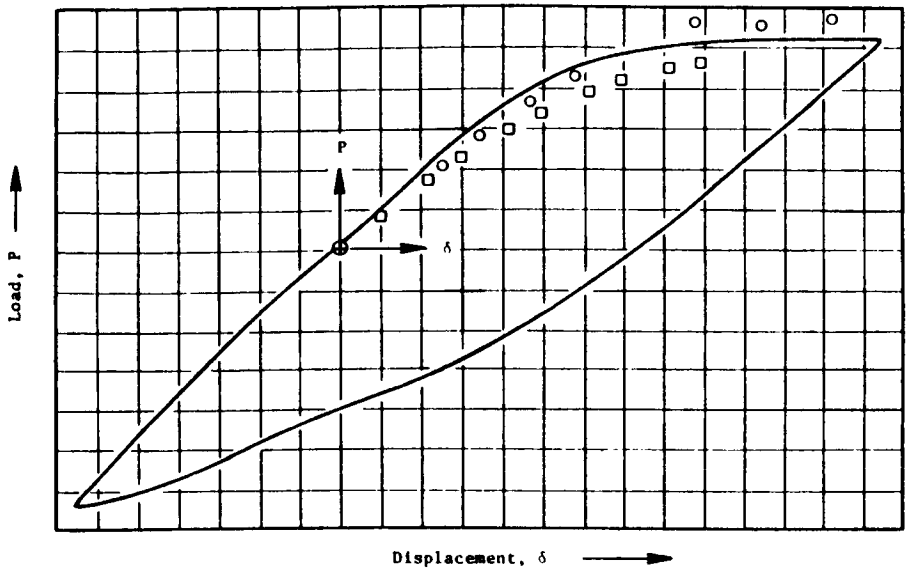

Figure 5. Load Versus Displacement Plot at Middle (X = 0.2 in.) Extenometer Location in the Gage Section of the SEN Specimen at Y = 0.28 inch.

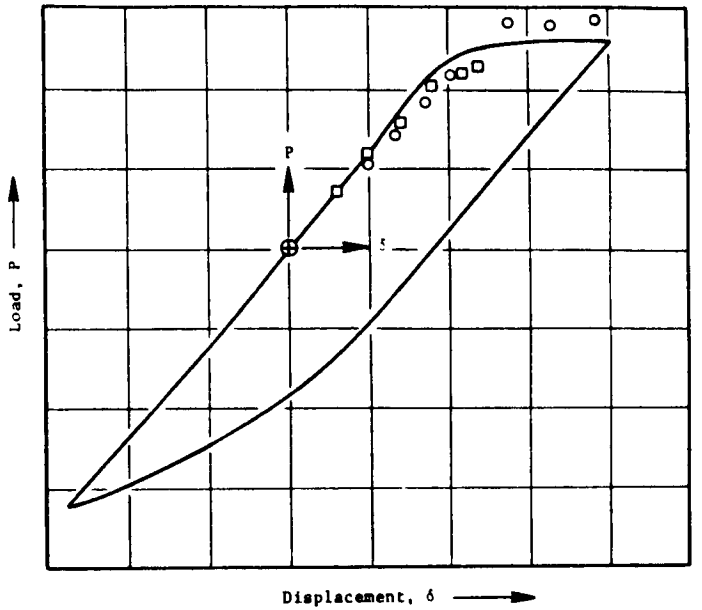

Figure 6. Load Versus Displacement Plot at Back-Face (X = 0.4 in.) Extensometer Location in the Gage-Section of the SEN Specimen at Y = 0.28 inch.

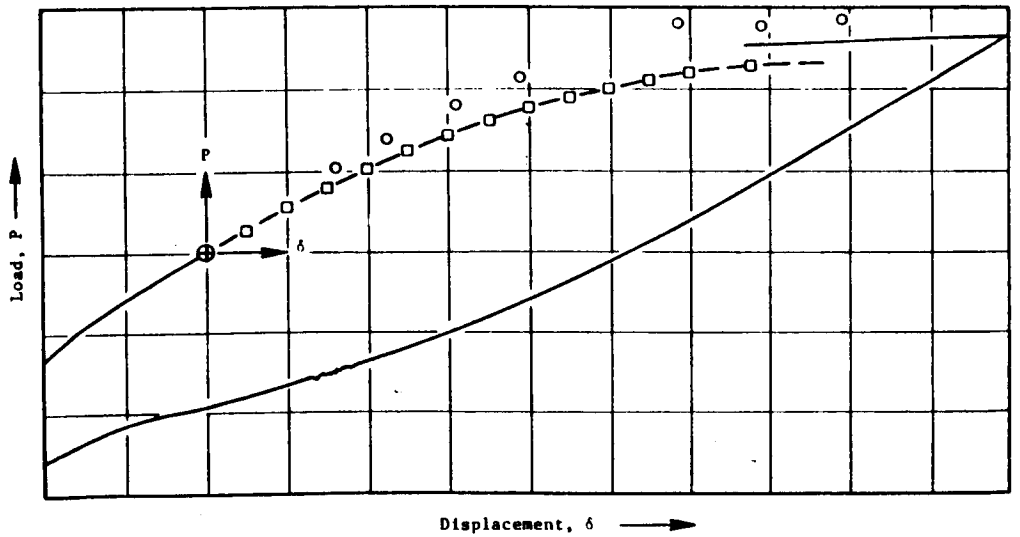

Figure 7. Load Versus Displacement Plot at Front-Face (X = 0.0 in.) Extensometer Location in the Gage - Section of the SEN Specimen at U = 0.28 inch.

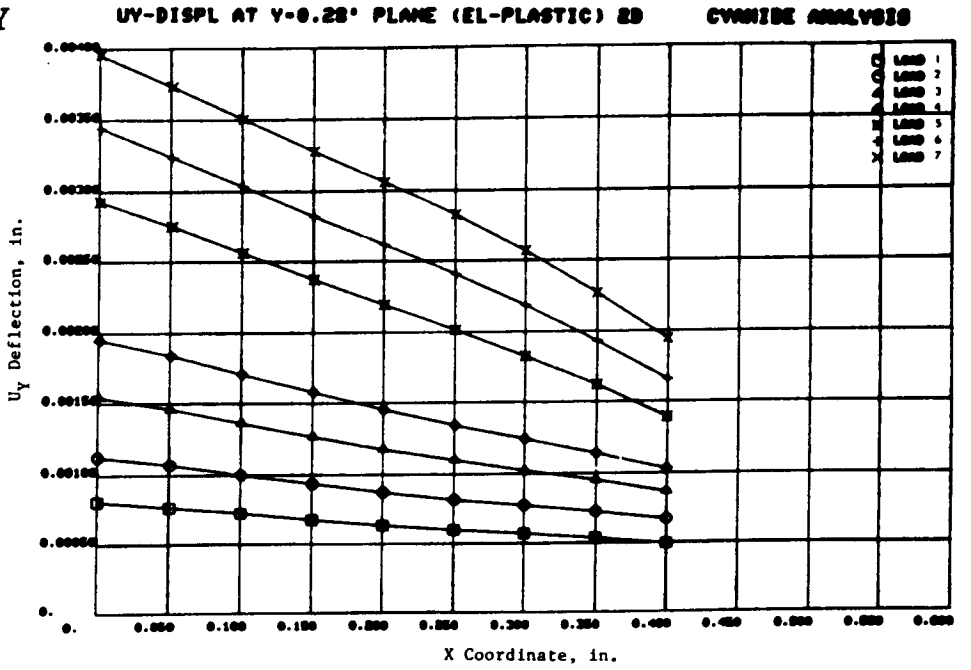

Figure 8. Normal Displacement U_Y at Y = 0.28 inch Plane in Gage-Section as a Function of Specimen Width for the Seven Applied Displacement Cases.

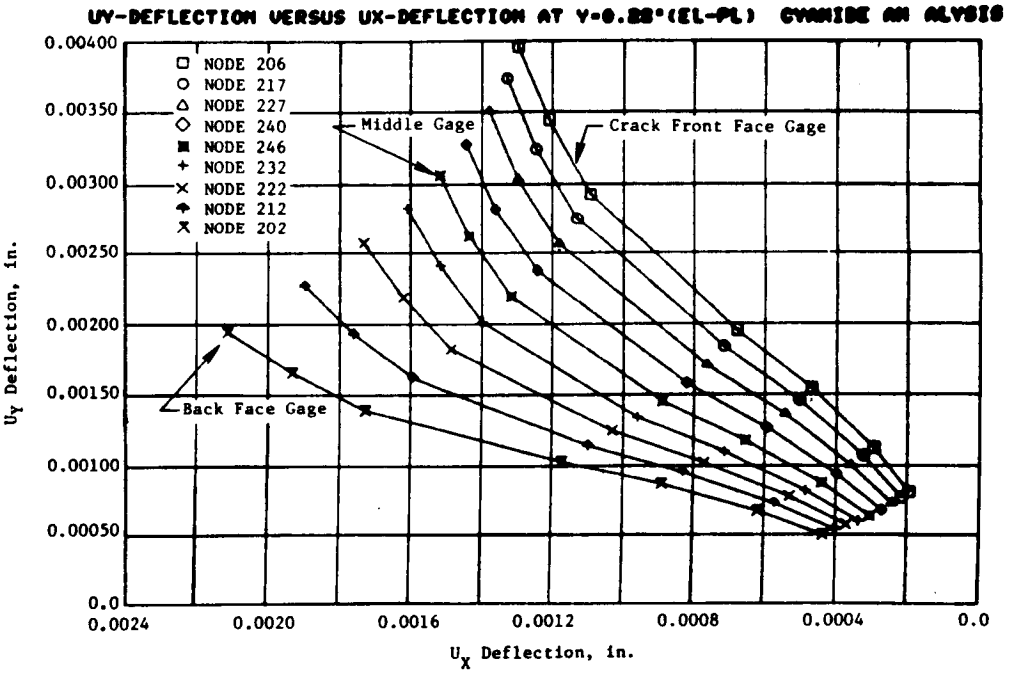

Figure 9. U_Y Versus U_X Displacement Curves at Each of Nine Locations on Y = 0.28 inch Plane in Gage - Section for the Seven Applied Displacement Cases.

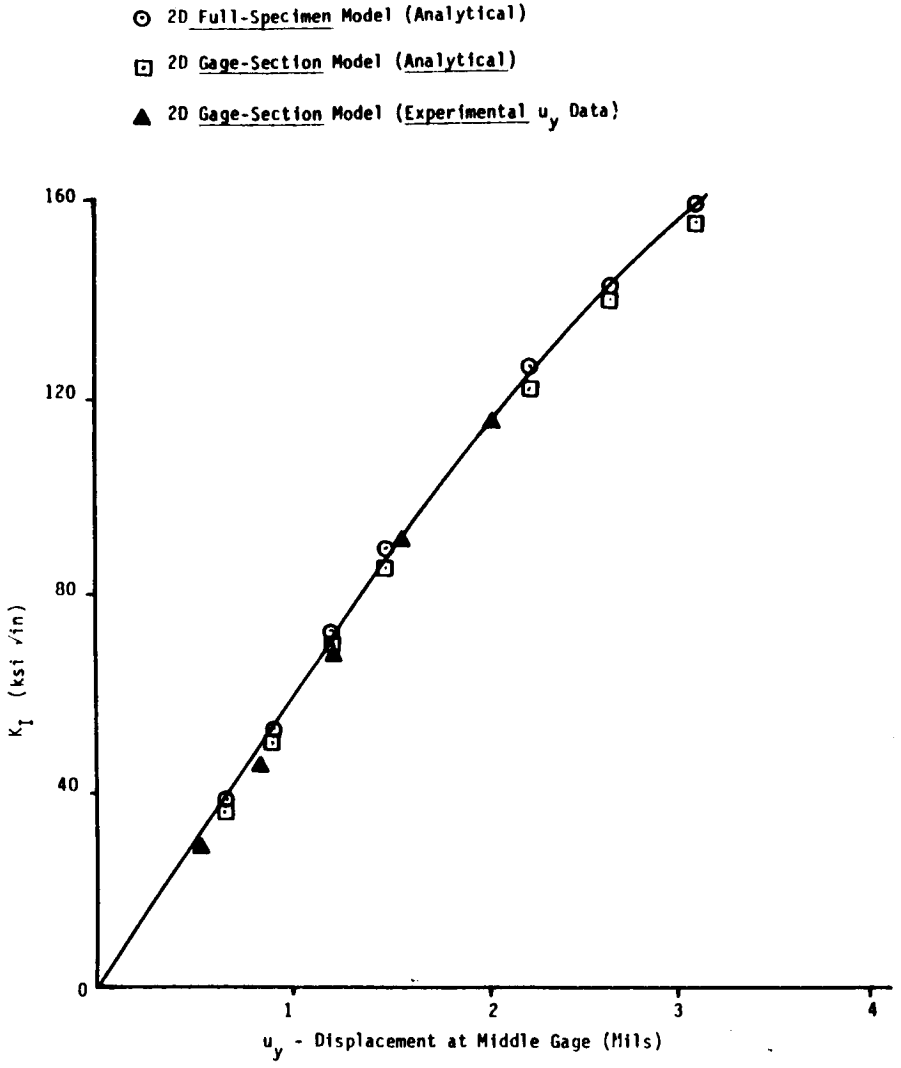

Figure 10: Vertical Displacement Boundary Condition Simulation in Terms of Elastic-Plastic Stress Intensity Factor ($K_I = \sqrt{EJ_I}$) In the SEN Buttonhead Specimen (a/w = 0.265)

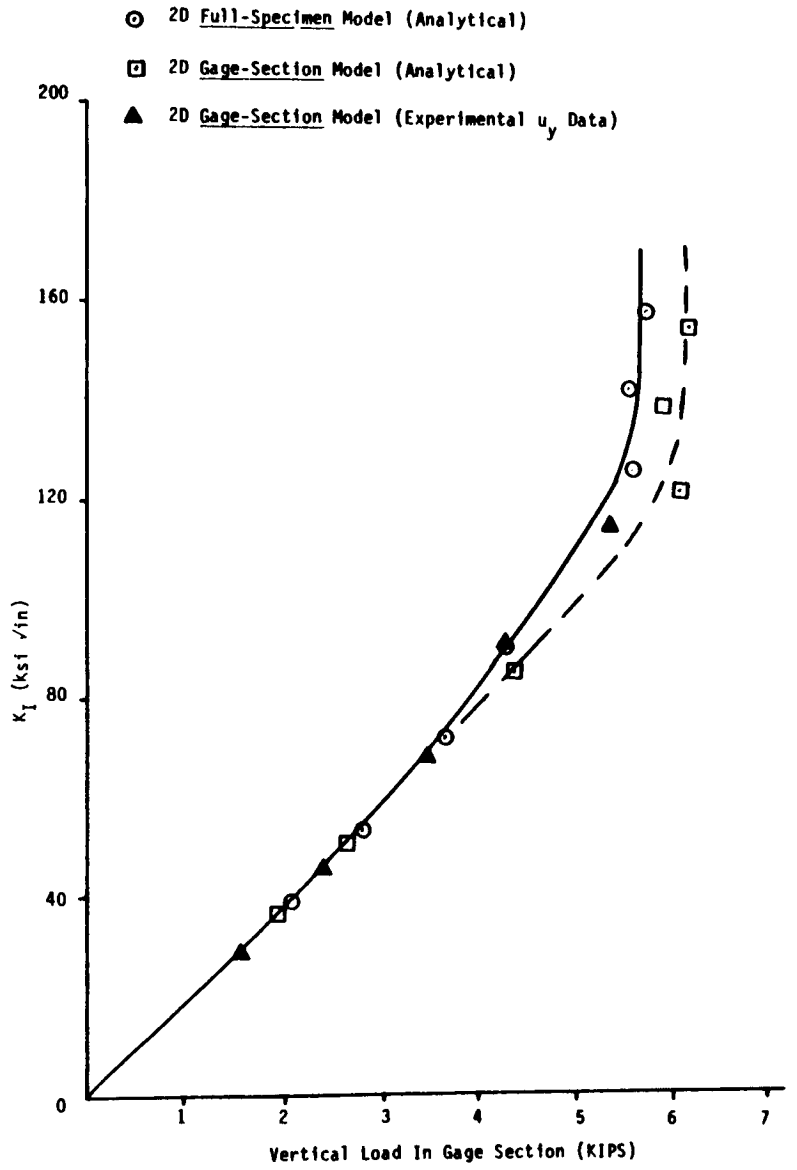

Figure 11: Stress Intensity Factor (K_I) In the Buttonhead SEN Specimen as a Function of Vertical Displacement Boundary Condition Induced Vertical Load (a/w = 0.265)